Jurnal Teknologi

Full Paper

CLASSIFICATION OF LUNG DISEASES FROM CHEST X-RAY IMAGES USING MODIFIED HOMOMORPHIC FILTERING AND HYBRID GLCM-MORPHOLOGY

Ahmed Sabeeh Yousif[a], Zaid H. Alsawaff[b], Zaid Omar[c]*

[a]Technical College of Management/Mosul, Northern Technical University, Mosul, 41001, Iraq
[b]Department of Medical Instrumentation Technology, Technical Engineering College, Northern Technical University Mosul, Iraq.
[a,b]Center of Technical Research, Mosul, Northern Technical University Mosul, Iraq, 41001
[c]Faculty of Electrical Engineering, Universiti Teknologi Malaysia, 81310 UTM Johor Bahru, Johor, Malaysia

Article history
Received
14 June 2025
Received in revised form
7 October 2025
Accepted
14 October 2025
Published Online
16 June 2026

*Corresponding author
zaidomar@utm.my

Graphical abstract

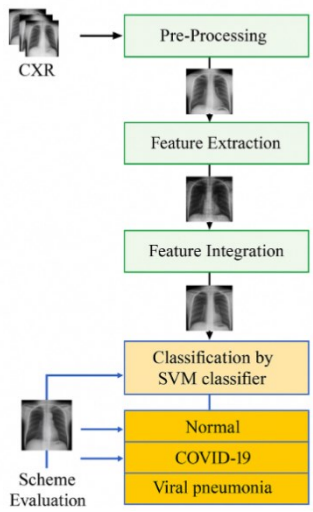

Abstract

Infectious diseases such as Coronavirus disease (COVID-19), viral pneumonia, and other pulmonary conditions continue to significantly affect people, leading to a high number of deaths in populations worldwide. Early testing and diagnosis are essential for improving patient outcomes within the healthcare system. This paper introduces a new classification framework, namely MHF-GM, which combines Modified Homomorphic Filtering (MHF) with a hybrid Gray Level Co-occurrence Matrix (GLCM) and a morphological feature extraction scheme for chest X-ray (CXR) images. The proposed MHF enhances image quality by incorporating a directional filter emphasizing diagonal features critical for diagnostic analysis. Key features, including texture descriptors (contrast, correlation, energy, homogeneity) and morphological parameters (area and perimeter), are integrated into a unified feature vector. A Support Vector Machine (SVM) is employed to differentiate between normal, viral pneumonia, and COVID-19 CXR images. Experimental evaluations on a dataset of 3,000 images across multiple classes show the superiority of our proposed method, achieving a classification accuracy of up to 98% in the training and testing stage by split the whole data to 70/30 for input images, thereby outperforming conventional techniques in terms of image enhancement and diagnostic performance. The findings underscore the effectiveness of the MHF-GM-based hybrid approach as a robust and cost-efficient solution for automating lung disease classification in clinical settings.

Keywords: Homomorphic Filtering, GLCM, Morphological Operation, Chest X-Ray, SVM

Abstrak

Jangkitan seperti penyakit koronavirus 2019 (COVID-19), pneumonia virus dan gangguan paru-paru lain terus menyumbang kepada kadar kematian yang tinggi di seluruh dunia. Pengesanan serta diagnosis awal amat penting untuk memperbaik hasil klinikal. Kajian ini memperkenalkan MHF-GM, iaitu kerangka klasifikasi yang menggabungkan Penapisan Homomorfik Terubah Suai (MHF) dengan ciri tekstur hibrid Matriks Kejadian Tahap Kelabu (GLCM) serta ciri morfologi bagi imej sinar-X dada (CXR). Komponen MHF menambah baik kualiti imej menggunakan penapis berarah yang menyerlahkan struktur pepenjuru yang relevan untuk tujuan diagnostik. Vektor ciri dibentuk dengan menghimpunkan deskriptor

tekstur (kontras, korelasi, tenaga, homogeniti) bersama parameter morfologi (luas, perimeter), manakala pengelasan dilakukan menggunakan Mesin Vektor Sokongan (SVM) kepada tiga kategori: normal, pneumonia virus dan COVID-19. Ujian ke atas 3,000 imej dengan pembahagian latih–uji 70/30 menunjukkan ketepatan sehingga 98%, mengatasi pendekatan konvensional dari segi penambahbaikan imej dan prestasi diagnostik. Dapatan ini menunjukkan bahawa MHF-GM merupakan penyelesaian automasi yang teguh serta kos-efektif untuk pengelasan penyakit paru-paru dalam persekitaran klinikal.

Kata kunci: Penapisan Homomorfik, GLCM, Operasi Morfologi, Sinar-X Dada, SVM

1.0 INTRODUCTION

X-ray chest examinations have been clinically important in the detection and monitoring of the progression of various pulmonary conditions, including emphysema, chronic bronchitis, pulmonary fibrosis, cancer of the lungs, and pneumonia [1-3]. The infectious coronavirus disease, or COVID-19, is caused by severe acute respiratory syndrome coronavirus 2 (SARS-CoV-2). After its initial identification in December 2019 in Wuhan, Hubei Province, China, its swift global expansion led to a worldwide pandemic [1]. By October 15, 2021, nearly 240 million confirmed infections had been recorded, with 4.8 million dying due to COVID-19, according to the Johns Hopkins University COVID-19 Dashboard [2]. Fever, extreme tiredness, shortness of breath, and loss of taste and/or smell are some of the primary symptoms [3].

A vital aspect of modern healthcare is the capacity to diagnose lung diseases quickly and accurately through radiographic imaging. This could considerably boost outcomes for patients due to early detection and treatment. Being widely available and cost-effective, X-ray imaging is still a mainstay when initially screening and diagnosing several pulmonary conditions. These include pneumonia, tuberculosis, cancer of the lungs, and complications induced by COVID-19 [4]. However, radiology expertise is widely relied on when interpreting the resulting images, which can entail variability and oversight. This applies especially when the case volume is high or there is a scarcity of specialist resources. Consequently, there is a burgeoning interest in developing advanced computational methods that can support and augment the diagnostic process [5].

The infection can result in major respiratory complications, principally pneumonia, in certain instances, which require the patient to be hospitalised and often admitted to intensive care units (ICU). However, due to the unfortunately limited ICU ward capacity, the volume of cases has overwhelmed numerous healthcare systems [6]. At the pandemic's peak, many countries established severe physical distancing policies, such as nationwide lockdowns. Real-time reverse transcription polymerase chain reaction (RT-PCR) is the primary tool for diagnosing COVID-19. Chest X-ray (CXR) and computed tomography (CT) scanning are often used in clinical practice to screen for the detection of COVID-19 pneumonia. CXRs are cost-effective and enable a bedside assessment of a patient's lungs, hence their long-standing usage as a portable tool [7].

Therefore, greater attention has recently been devoted to the development of artificial intelligence-based (AI) methods involving the automated detection of COVID-19 pneumonia using CXR imagery. Approaches involving deep learning have been especially investigated and suggested as image processing solutions that are efficient and driven by data [8]. Medical applications have featured in this research [9–11].

RT-PCR quantification has low sensitivity, so it is prone to a high rate of false negatives. This makes it hard to offer a COVID-19 infection diagnosis with confidence, affecting infected patients' timing of treatment and disposition. Meanwhile, when evaluating the clinical course of COVID-19, a vital aspect can be radiological imaging (CXR and CT), which is also critical in the subsequent selection of suitable patient management. Whereas a CT scan is regarded as the diagnosis gold standard, as demonstrated by Saleh *et al*. [12, 13], the use of a digital CXR system remains especially applicable when diagnosing and treating emergencies. This is due to its speed, ease of use, relative lost cost, widespread availability, and capacity to deliver doses of lower radiation.

A new drive is stimulating computer-assisted screening and diagnosis due the emergence for the digital chest radiography with, the potential of digital image processing. In recent times, several methods for segmenting CXR images and extracting lung boundary have been proposed, based on various methodologies. Firstly, methods based on rules mainly approximate their solutions using heuristic assumptions. These figures can serve as start values for other, the more robust schemes for segmentation. Saad *et al*. has suggested a scheme for segmentation of lung places in CXR scan images using a Canny-edge detector coupled with morphological operators [14]. As a general scheme meanwhile involves classifying pixels through modeling the regions around the lungs and marking them into either object or background.

Subsequently, there have been methods that are based on modelling the lungs' shape or appearance [15]. In addition to these, researchers also use a combination of methods. For example, Li *et al*. [16] advocated the use the graph based segmentation scheme through saliency information, basing this on a global contrast function. Jaeger *et al*. [17] merged graph cut optimization scheme and a method of the lungs. Meanwhile, hybrid methods are developed to improve results through fusion of multiple techniques. In [18], Jaeger *et al*. devised an approach for extracting the lung region, which involved the combination of an intensity mask, a lung model mask derived from training on a dataset, and a Log-Gabor mask. However, despite its pervasiveness in the medical field, standard CXR remains a complicated imaging instrument.

Hassanien *et al*. [19] presented a methodological proposal to classify COVID-19 lungs automatically via X-rays by utilising an Otsu algorithm-based multi-level threshold and the support vector machine for the task of predicting. In another work, Hammoudi *et al*. [20], presented a proposal for a strategy based on deep learning that would automatically detect if chest X-ray images were healthy or showed bacterial or viral pneumonia. The assumption was that COVID-19-infected patients subjected to testing during an epidemic were highly likely to be true positives when the classification results indicated a virus.

A review of the related studies indicated the need to identify various challenges related to the classification of lung diseases utilising CXR imagery.

Problem.1: CXR images fail to provide high resolution, resulting in low contrast and illumination problems that lead to unclear lung boundaries. Consequently, radiologists face significant challenges in reading and analyzing disease formations.

Problem .2: Different of lung diseases, for instances: viral infections and COVID-19, are considered dangerous cases for human life; therefore, classifying and detecting each disease with high-performance evaluation with assessment metrics for instances; accuracy, F1-score, and recall is of utmost importance.

In consideration of the above, the main contributions of this paper can be summarized as follows:

1. A modified scheme for the pre-processing stage that enhances the contrast and illumination of CXR images using modified Homomorphic filtering, particularly emphasizing diagonal structures critical for diagnostic analysis. The novelty lies in presenting a directional high-pass filter component that improves the visibility of diagnostic features and addresses low contrast in output images.
2. The first application of integrating gray level co-occurrence matrix (GLCM) with texture features (correlation, energy, contrast, and homogeneity) and morphological features (area and perimeter) to create a comprehensive feature set. The proposed feature integration approach captures both texture and structural characteristics of different lung diseases, which is essential for accurate disease classification.
3. The methodology provides clear interpretation of results through an explainable MHF-GM-based support vector machine classification to support clinician decision making.

Overall, our method combines Modified Homomorphic Filtering (MHF) with a hybrid GLCM and morphological feature extraction scheme for CXR images. The proposed MHF first enhances image quality by incorporating a directional filter that emphasizes diagonal features critical for diagnostic analysis. The method then combines GLCM with texture features alongside morphological features to create feature vectors. An SVM-based classifier is then used to classify CXR images into three classes: viral pneumonia, COVID-19, and normal. This study's main objective was to form a new framework that could classify multiple lung disease classes with speed and accuracy using few parameters, including various sizes of dataset and resolution. This would demonstrate that the framework was suitable for authentic application without the need for major computational resources. Because deep- learning needs large curated data and can fail under domain shift, this paper use a hybrid of modified homomorphic filtering, GLCM, and morphology to provide a practical, interpretable alternative.

2.0 METHODOLOGY

2.1 Overview

Computer-aided diagnosis/detection (CAD) and classification aim to help clinical experts evaluate the various structures and shapes from chest X-Ray (CXR), and thus its abnormalities [15-20]. The configuration and dimension of the lungs can reveal indicators of severe conditions, including pneumothorax, pneumoconiosis, and emphysema, as well as COVID-19 and viral pneumonia. Our work aims to assist in decision-making to estimate the presence of these different pathologies. Figure 1 refer to the outline of the proposed method.

2.2 Pre-processing

The technique of homomorphic filtering [21,22] is deployed in signal processing to support imagery degraded by factors like noises, illuminations, or contrast. The basis of this approach is to divide images $f(x,y)$ into illumination $f_l(x,y)$ and reflectance $f_r\ (x,y)$ elements. The former describe the light intensity and type that shines on scenes or objects, while the latter

represent the intrinsic attributes of objects or scenes themselves. The relationship between the image and these components can be expressed with the following model:

$$f\ (x,y)\ =\ f_l(x,y)\ .f_r\ (x,y) \qquad (1)$$

The advantage of our proposed modified homomorphic filtering is to allow for customized enhancement capabilities, potentially providing better visibility of features with specific orientations, which can be especially useful in medical imaging, where the directionality of textures and structures may carry diagnostic significance. The following steps describe the modified homomorphic filtering:

Step 1: Apply the transformation:

$$m(n,m)=\ Log\ (1+f(n,m)) \qquad (2)$$

Step 2: Perform Fourier Transform:

$$P(k,l)=\ \mathbb{F}\ \{m(n,m)\} \qquad (3)$$

Step 3: Apply a directional High-pass Filter. This combines high- and low-pass attributes with a directional element to emphasize a particular direction, such as the diagonal:

$$D(k,l)=\left(1-e^{-\frac{H^2(k,l)}{2\sigma_{low}^2}+-\frac{H^2(k,l)}{2\sigma_{high}^2}}\right).DirComp(k,l) \qquad (4)$$

where σ_{low} and σ_{high} refer to the parameters that define the cutoff frequencies for the low-pass and high-pass, and $DirComp(k,l)$ represents the directional component that emphasizes certain directions in the frequency domain. It has been designed to enhance features with specific orientations, particularly diagonal ones.

Step 4: Perform inverse Fourier Transform:

$$y(n,m)=\mathbb{F}^{-}\{P(k,l).D(k,l)\} \qquad (5)$$

Step 5: Finally, perform the exponential transformation:

$$f'(n,m)=\ e^{h(n,m)}-1 \qquad (6)$$

The novelty of the proposed homomorphic filter lies in Step 3, where the directional component $DirComp(k,l)$ was designed to focus on features adapted to the orientation. The method enhances diagonal directions, which is achieved by multiplying the two high- and low-pass filter components with the directional factor.

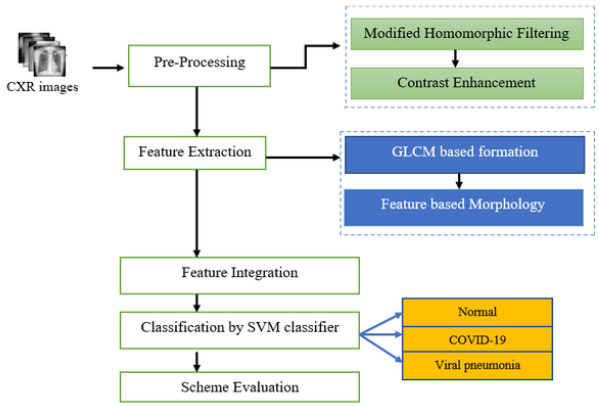

Figure 1 Outline the proposed MHF-GM for the classification of CXR images

A comparison of the suggested filter versus traditional homomorphic filters is as follows:

1. The unique use of $\tan^{-1}(y,x)$ to calculate the angle and subsequently create a filter that emphasizes diagonal features through $abs(cos(\theta)\ \times\ sin(\theta))$.

   $$Dircomp(k,l)=|\cos\theta\sin\theta| \qquad (7)$$

   where $\theta=tan^{-1}(\frac{l}{k})$ refers to the angle of the point (k,l) in the frequency domain. cos θ and sin θ refer to the orientation of the features in the CXR images.

2. Therefore, our method potentially enhances the visibility of diagonal structures in the image, which can be crucial for detecting certain conditions in radiographic images or enhancing textures in a way that traditional homomorphic filters may not.

3. The filter combines the characteristics of the high-pass and low-pass with the directional component. This hybrid approach not only enhances contrast by managing frequencies differently but also in a direction-sensitive manner, which is not commonly seen in standard homomorphic filtering techniques.

$$H_{combined}\ =H_{high}(k,l).H_{low}(k,l).DirComp(k,l) \qquad (8)$$

where $H_{high}(k,l)$ presents the high-frequency components – edges and fine structure, while $H_{low}(k,l)$ refers to the low-frequency parts such as illumination, and $DirComp(k,l)$ is the orientation structure.

2.3 Proposed Feature Extraction

2.3.1 Gray Level Co-occurrence Matrix

GLCM-based feature extraction quantifies the frequency of specific combinations of gray-level intensities occurring in an image, thereby capturing textural characteristics. This method provides valuable descriptors such as contrast, correlation, energy, homogeneity, area, and perimeter [23]. The mathematical formulation of each feature is presented below:

1. Contrast

Contrast is used to measure the difference in intensity between pixels and their neighbours across a complete image. It measures local variations within images.

$$Contrast = \sum_{i=0}^{N_g-1}\sum_{j=0}^{N_g-1}(i-j)^2 p(i,j) \quad (9)$$

Where i, and j are the pixel intensity values, and $p(i,j)$ is the GLCM at value (i,j). Also, N_g is the number of gray levels in the images.

2. Correlation

Correlation measures the linear dependency of gray levels on those of neighboring pixels.

$$Correlation = \frac{\sum_{i=0}^{N_g-1}\sum_{j=0}^{N_g-1}(i-\mu_i)(j-\mu_j)P(i,j)}{\sigma_i\sigma_j} \quad (10)$$

3. Energy

Energy, also referred to as the Angular Second Moment, represents the sum of the squared values within the GLCM. It reflects the uniformity of texture in the image, with higher values indicating more consistent texture patterns

$$Energy = \sum_{i=0}^{N_g-1}\sum_{j=0}^{N_g-1} P(i,j)^2 \quad (11)$$

4. Homogeneity

Homogeneity, also known as the Inverse Difference Moment, evaluates how closely the GLCM elements are distributed along its diagonal. Its value diminishes as the disparity between neighboring gray levels grows.

$$Homogeneity = \sum_{i=0}^{N_g-1}\sum_{j=0}^{N_g-1}\frac{P(i,j)}{1+|i-j|} \quad (12)$$

5. Area and Perimeter

The parameters area and perimeter are not directly defined in the context of GLCM, but in image processing these refer to the region of interest (ROI) in the spatial domain, rather than the GLCM domain. Area refers to the number of pixels that constitute the object or region, while perimeter is the total length of the boundary of the object or region.

2.3.2 Morphological Features

Morphological features [24] such as area and perimeter are extracted from binary images using the following steps:

1) Binary Conversion:

$$BW = imbinarize\ (I, threshold) \quad (13)$$

where I is the grayscale image and threshold is the selected threshold level for binarization.

2) Closing process:

$$BW_{close} = imclose(BW, SE) \quad (14)$$

where SE is the structuring element.

3) Area and Perimeter:

$$Area = \sum pixels\ within\ the\ connected\ component \quad (15)$$

$$Perimeter = boundary\ length\ of\ connected\ component \quad (16)$$

After applying the closing operation, connected components i.e. regions of adjacent white pixels are identified. The ROI is then utilized to estimate the area (number of pixels in the region) and perimeter (the boundary length of these regions).

2.4 Feature Integration

Various features that apply texture through GLCM and shape through morphological analysis are integrated into a single classifier. Once extracted, features are merged into a single feature vector for each image. Here SVM is used in our paper as shown below:

$\min_{s,v}\frac{1}{2}\|W\|^2$ which is subject to $y_i(W.F_i + b) \geq 1$ (16)

where W is the weight vector, b is the bias, and y_i refer to the class label for feature vector P_i.

$$P_i = [C_i, Co_i, E_i, H_i, A_i, P_i] \quad (17)$$

P_i represents the contrast, correlation, energy, homogeneity, area, and perimeter respectively. These feature vectors are then organized into a matrix for all images:

$$\text{Feature vector} = \begin{bmatrix} c1 & \cdots & p1 \\ \vdots & \ddots & \vdots \\ C_n & \cdots & p_n \end{bmatrix} \quad (18)$$

3.0 RESULTS AND DISCUSSION

The primary aim of this study is to evaluate the effectiveness of the proposed model in differentiating between COVID-19, viral pneumonia, and normal

chest X-ray (CXR) images, given that both COVID-19 and viral pneumonia are viral in origin and exhibit overlapping radiographic features. The dataset used for experimentation is described in [6]. Features were standardized through z-score normalization, with the mean and variance estimated on the training split; the identical transform was then applied to the validation and test sets. This Paper segmented a binary ROI via Otsu's criterion on the MHF output, cleaned it with opening (3-px disk) and hole filling, then computed features only inside the ROI.

The highest possible image count related to three classes of lung disease is 3000 CXR images; these contain normal, viral pneumonia, and COVID-19. Since COVID-19 is also influenced by a virus, viral pneumonia was also considered. Therefore, the proposed scheme was used to test its model evaluation in differentiating viral pneumonia from COVID-19 CXR lung images. Input images were partitioned samples (70/15/15; no overlap) with stratification to maintain class balance and acquisition diversity. The Performance variability was assessed through 5-fold stratified CV on the training split, reporting fold-averaged results.

The experiments in this study were performed using a MATLAB-based framework on a system equipped with an Intel Core i9 processor, a dedicated GPU, 32 GB of RAM, and running Windows 10 Pro, and the input image was used with size 128×128. Figure 2 shows the samples of CXR images for different lung disease classifications: Normal, COVID-19, and Pneumonia.

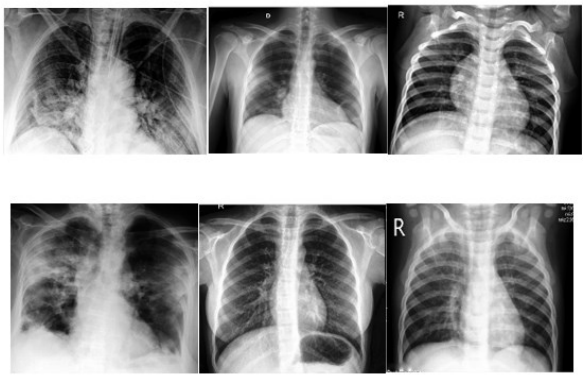

Figure 2 Samples of clinical image data with low contrast and illumination for multiple cases of lung disease such as No Finding, COVID-19, and Pneumonia

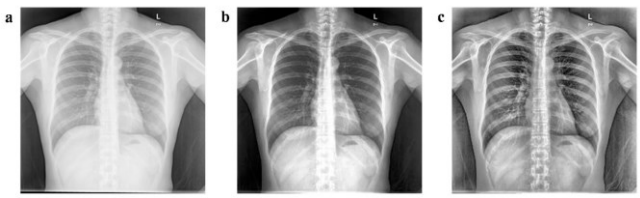

Figure 3 (a) Normal image; (b) The outcome of a classic filter; (c) The result of introduced modified filter enhancement

Table 1 Performance analysis of the proposed enhanced CXR images using a modified filter

Images	PSNR (db)	AMBE	EME	FSIM
Set A	33.3	1.63	16.22	0.89
Set B	40	2.74	22.59	0.96
Set C	31.5	3.44	9.58	0.88
Set D	38.3	2.22	18.66	0.94
Set E	39	5.4	20.77	0.93
Set F	44	5.12	11.89	0.98

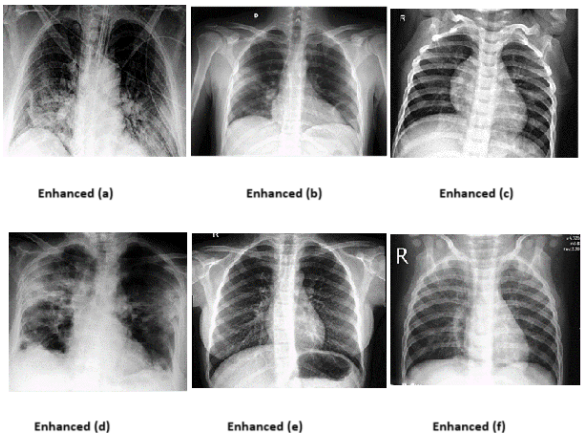

Figure 4 The enhancement results for sets a, b, c, d, e, and f, as shown in Figure 2, were obtained using the proposed Modified Homomorphic Filtering (MHF) method

a. Trial 1: Enhance CXR images using the proposed MHF scheme

Table 1, and Figure 3 shows the performance evaluation, with the proposed scheme's effectiveness measured through several metrics. The Entropy-based Measure of Enhancement (EME) was used, where higher EME values indicate better enhancement. The Absolute Mean Brightness Error (AMBE) was calculated to evaluate brightness preservation, with lower AMBE values reflecting better performance. The Peak Signal-to-Noise Ratio (PSNR) was measured in decibels (dB) to determine the visual quality of the enhanced image; values above 30(dB) are considered acceptable. Lastly, the similarity between the initial and enhanced imagery was compared using the Feature Similarity Index Measurement (FSIM), the values for which range between -1 and +1. For optimal results, FSIM should be close to +1 [25, 26].

Table 2 Performance comparison of the proposed method MHF over the state of arts

Methods	Metric			
	PSNR (db)	AMBE	EME	FSIM
[27]	33.3	1.63	16.22	0.89
[28]	40	2.74	22.59	**0.96**
Proposed MHF	**44.5**	**3.44**	**9.58**	0.94

Several experiments were conducted to compare the proposed MHF scheme with those in [27] and [28], with the same CXR images being utilized. Table 2 highlights the performance metrics EME, AMBE, PSNR, and FSIM for a total of 100 low-contrast illumination of CXR images. Figure 2 meanwhile demonstrates the six sets for three categories Normal, COVID-19, and Viral Pneumonia. According to both Table 2 and Figure 4, MHF has shown superior performance based on different metrics compared to recent other works. Good scores were recorded for PSNR, AMBE, FSIM, and EME, denoting its ability to discern the details of the enhanced images, preserving a higher visual quality index, and brightness and leading to moderate contrast illumination of CXR image.

b. Trial 2: Binary classification between No-Finding and COVID-19

The provided enhanced CXR images are then fed as input to the trained SVM and the final outputs are estimated using the aforementioned metrics: Accuracy, Precision, Recall, and F1 score [29].

Table 3 Support Vector Machine (SVM) class-wise classification results for COVID-19 detection in Trial 2

Disease name	Precision	Recall	F1-Score	Accuracy (%)
Normal	0.97	0.99	0.96	0.95
COVID-19	0.95	0.92	0.93	0.99
Average	0.96	0.95	0.94	0.96

Various research has tested the recent works in terms of binary classification as compared to multi-class classification [30, 31]. From Table 3, MHF has been evaluated using two classes comprising 125 CXR images of normal patients and 75 COVID-19 cases for the training stage. The accuracy-based metric of the proposed framework recorded 95% and 99%, respectively, while the average is 96%. The average precision, recall, and F1-score also showed better performance with averages of 96%, 95%, and 94% as seen in Table.3.

c. Trial 3 Binary classification between No-Finding and Viral Pneumonia

Table 4 Class-wise classification performance of SVM in Trial 3.

Disease name	Precision	Recall	F1-Score	Accuracy (%)
Normal	0.98	0.97	1.00	0.99
Viral pneumonia	1.00	0.99	0.98	0.94
Average	0.99	0.98	0.99	0.96

Here, we again utilize binary classification. From Table 4, MHF has been evaluated using two classes comprising 125 CXR images of normal patients and 75 viral pneumonia cases for the training stage. The proposed framework achieved an average accuracy of 96%, with precision, recall, and F1-score averaging 99%, 98%, and 99%, respectively, as presented in Table 4.

d. Trial 4: Multi-class classification with No-Finding, COVID-19, and Viral Pneumonia

Table 5 Support Vector Machine (SVM) class-wise performance in detecting the three classes in Trial 4.

	Precision	Recall	F1-Score	Accuracy (%)
Normal	0.88	0.98	0.94	1.00
Viral pneumonia	0.95	0.93	0.95	0.98
COVID-19	0.99	1.00	0.95	0.99

In the current trial, the performance of the model in terms of precision, recall, F1-score, and accuracy was identified using 2000 CXR images (normal: 1090, viral pneumonia: 410, and COVID-19: 500), which Table 5 illustrates. It was noticed, compared to recent works [32, 33], that the results showed superior performance with an average of around 98% for the classification of three classes. As a result, we conclude that the proposed scheme has successfully demonstrated its discriminant ability to classify COVID-19.

Table 6 Benchmark comparison of the proposed method over the state of the art

Methods	#-classes	Precision	Recall	F1-Score	Accuracy (%)
Khan *et al*, 2020 [30]	**2**	93%	97.2%	90%	89.9%
Rahman *et al*, 2020 [31]	**2**	98.57%	98.56%	95%	98.60%
Randieri *et al*, 2021 [32]	**3**	94.6 %	95.24%	94%	**98.22%**
Oltu *et al*, 2021 [33]	**3**	94 %	96.21	91.2	94.1%
Proposed MHF-GM-SVM	**3**	95.6%	**100%**	95%	99%
Proposed MHF-GM-SVM	**2**	**99%**	98%	**99.2%**	96%

In Table 6, a comparison was made to evaluate the proposed enhanced CXR-based hybrid (GLCM) and morphological feature extraction scheme (MHF-GM) against state-of-the-art methods [30-33]. Performance metrics, including precision, recall, F1-Score, and accuracy, were used for the evaluation. The same datasets were utilized, employing both two-class and three-class classifications, with standardized settings to perofor the validate of robustness for the proposed scheme.

Table 6 demonstrates the superior performance of our proposed method. For instance, the proposed MHF-GM achieved higher metrics when classifying lung diseases into two classes: Accuracy = 96%, Recall = 98%, F1-Score = 99%, and Precision = 99%, outperforming the work in [30]. Similarly, for three-class classification, the proposed MHF-GM achieved equally high results: Accuracy = 99%, Recall = 100%, and F1-Score = 95%, although it fell short in maintaining a high Precision (95.6%). This decrease in Precision is likely due to challenges in distinguishing subtle features and overlapping problems within the dataset, which can lead to slight reductions in the metric. Dataset size and single-centre source; despite patient-wise splits, multi-site external validation and matched comparisons with recent deep models are still needed. Next: multi-centre/prospective tests, uncertainty calibration, domain-shift adaptation, and benchmarking against strong CNN/transformer baselines. Finally, For the fair comparison, the paper has been tested them to compare (i) HF scheme : Which features estimated on the full MHF-enhanced image, over the (ii) HF with ROI scheme : the same scheme but features restricted to the binary ROI, it was seen that the HF+ROI is shown good resultant compare to the HF scheme (i.e: accuracy= 95%) for the test images.

4.0 CONCLUSION

The study introduced a novel MHF-GM scheme that accurately detects various life-threatening lung diseases by classifying chest X-ray (CXR) images using a machine learning-based SVM classifier, even with a limited dataset size. The proposed method combines Modified Homomorphic Filtering (MHF) with a hybrid Gray Level Co-occurrence Matrix (GLCM) and a morphological feature extraction scheme. This method was applied to a dataset of 3000 CXR images spanning three classes, which was curated by merging several available datasets.

Extensive trials were conducted, demonstrating strong performance metrics, including Precision, Recall, Accuracy, and F1-Score, with values of 0.98 or higher, outperforming other recent methods. The study also demonstrated that the proposed MHF-GM scheme can reliably classify COVID-19 cases. Furthermore, it outperforms existing multiclass and binary classification schemes in terms of various evaluation metrics.

Accurate classification and complementary information from CXR images of lung diseases play a crucial role in achieving full automation in medical and clinical diagnosis. Moreover, the proposed scheme can also potentially be utilized as a decision support system for clinical specialists, aiding in accurate and timely decision-making.

Acknowledgement

The authors gratefully acknowledge their respective institutions for the academic and technical support provided throughout this study.

Conflicts of Interest

The authors confirm that there are no conflicts of interest associated with this publication.

References

[1] Cucinotta, D., and M. Vanelli. 2020. WHO Declares COVID-19 Pandemic. *Acta Bio-Medica: Atenei Parmensis*. 91(1): 157.

[2] Center for Systems Science and Engineering (CSSE), Johns Hopkins University. 2021. COVID-19 Dashboard. Accessed October 15, 2021. https://coronavirus.jhu.edu/map.html.

[3] Lauer, Stephen A., Kyra H. Grantz, Qifang Bi, Forrest K. Jones, Qulu Zheng, Hannah R. Meredith, Andrew S. Azman, Nicholas G. Reich, and Justin Lessler. 2020. The Incubation Period of Coronavirus Disease 2019 (COVID-19) from Publicly Reported Confirmed Cases: Estimation and Application. *Annals of Internal Medicine*. 172(9): 577–82. https://doi.org/10.7326/M20-0504.

[4] Wan Ahmad, Wan Siti Halimatul Munirah, Wan Mimi Diya Wan Zaki, Mohammad Faizal Ahmad Fauzi, and Wooi Haw Tan. 2016. Classification of Infection and Fluid Regions in Chest X-Ray Images. In *2016 IEEE International Conference on Digital Image Computing: Techniques and Applications (DICTA)*. 1–5. https://doi.org/10.1109/DICTA.2016.7797020.

[5] Candemir, Sema, Stefan Jaeger, Kannappan Palaniappan, Jonathan P. Musco, Rahul K. Singh, Zhiyun Xue, Alexandros Karargyris, Sameer Antani, George Thoma, and Clement J. McDonald. 2014. Lung Segmentation in Chest Radiographs Using Anatomical Atlases with Nonrigid Registration. *IEEE Transactions on Medical Imaging*. 33(2): 577–90. https://doi.org/10.1109/TMI.2013.2290491.

[6] Nahiduzzaman, M., M. O. F. Goni, R. Hassan, M. R. Islam, M. K. Syfullah, S. M. Shahriar, *et al.* 2023. Parallel CNN-ELM: A Multiclass Classification of Chest X-Ray Images to Identify Seventeen Lung Diseases Including COVID-19. *Expert Systems with Applications*. 229: 120528. https://doi.org/10.1016/j.eswa.2023.120528.

[7] Ieracitano, C., N. Mammone, M. Versaci, G. Varone, A. R. Ali, A. Armentano, and F. C. Morabito. 2022. A Fuzzy-Enhanced Deep Learning Approach for Early Detection of COVID-19 Pneumonia from Portable Chest X-Ray Images. *Neurocomputing*. 481: 202–15. https://doi.org/10.1016/j.neucom.2022.01.055.

[8] Gupta, R. K., N. Kunhare, R. K. Pateriya, and N. Pathik. 2022. A Deep Neural Network for Detecting Coronavirus Disease Using Chest X-Ray Images. *International Journal of Healthcare Information Systems and Informatics*. 17: 1–27. https://doi.org/10.4018/IJHISI.20220401.oa1.

[9] Marques, G., D. Agarwal, and I. de la Torre Díez. 2020. Automated Medical Diagnosis of COVID-19 through EfficientNet Convolutional Neural Network. *Applied Soft Computing*. 96: 106691. https://doi.org/10.1016/j.asoc.2020.106691.

[10] Das, D., K. Santosh, and U. Pal. 2020. Truncated Inception Net: COVID-19 Outbreak Screening Using Chest X-Rays. *Physical and Engineering Sciences in Medicine*. 43: 915–25. https://doi.org/10.21203/rs.3.rs-20795/v1.

[11] Rahman, T., M. E. Chowdhury, A. Khandakar, K. R. Islam, K. F. Islam, Z. B. Mahbub, *et al.* 2020. Transfer Learning with Deep Convolutional Neural Network (CNN) for Pneumonia Detection Using Chest X-Ray. *Applied Sciences*. 10(9): 3233. https://doi.org/10.3390/app10093233.

[12] Saleh, B. J., Z. Omar, V. Bhateja, and L. I. Izhar. 2023. Auto-Lesion Segmentation with a Novel Intensity Dark Channel Prior for COVID-19 Detection. *Journal of Physics: Conference Series*. 2622: 012002. https://doi.org/10.1088/1742-6596/2622/1/012002.

[13] Saleh, B. J., Z. Omar, M. A. As'ari, and V. Bhateja. 2024. Semi-Supervised Novel Radiomics Approach for COVID-19 Severity Detection Based on Atmospheric Veil Correction. In *2024 IEEE 8th International Conference on Signal and Image Processing Applications (ICSIPA)*. 1–6. Kuala Lumpur, Malaysia. https://doi.org/10.1109/ICSIPA62061.2024.10687266.

[14] Saad, Mohd Nizam, Zurina Muda, Noraidah Sahari Ashaari, and Hamzaini Abdul Hamid. 2014. Image Segmentation for Lung Region in Chest X-Ray Images Using Edge Detection and Morphology. In *2014 IEEE International Conference on Control System, Computing and Engineering (ICCSCE)*. 46–51. https://doi.org/10.1109/ICCSCE.2014.7072687.

[15] Xu, Tao, Mrinal Mandal, Richard Long, Irene Cheng, and Anup Basu. 2012. An Edge-Region Force Guided Active Shape Approach for Automatic Lung Field Detection in Chest Radiographs. *Computerized Medical Imaging and Graphics*. 36(6): 452–63. https://doi.org/10.1016/j.compmedimag.2012.04.005.

[16] Li, Xin, Leiting Chen, and Junyu Chen. 2017. A Visual Saliency-Based Method for Automatic Lung Regions Extraction in Chest Radiographs. In *2017 IEEE 14th International Computer Conference on Wavelet Active Media Technology and Information Processing (ICCWAMTIP)*. 162–65. https://doi.org/10.1109/ICCWAMTIP.2017.8301470.

[17] Jaeger, Stefan, Alexandros Karargyris, Sema Candemir, Les Folio, Jenifer Siegelman, Fiona Callaghan, Zhiyun Xue, Kannappan Palaniappan, Rahul K. Singh, Sameer Antani, George Thoma, Yi-Xiang Wang, Pu-Xuan Lu, and Clement J. McDonald. 2014. Automatic Tuberculosis Screening Using Chest Radiographs. *IEEE Transactions on Medical Imaging*. 33 (2): 233–45. https://doi.org/10.1109/TMI.2013.2284099.

[18] Jaeger, Stefan, Alexandros Karargyris, Sameer Antani, and George Thoma. 2012. Detecting Tuberculosis in Radiographs Using Combined Lung Masks. In *2012 Annual International Conference of the IEEE Engineering in Medicine and Biology Society*. 4978–81. https://doi.org/10.1109/EMBC.2012.6347110.

[19] Hassanien, A. E., L. N. Mahdy, K. A. Ezzat, H. H. Elmousalami, and H. A. Ella. 2020. Automatic X-Ray COVID-19 Lung Image Classification System Based on Multi-Level Thresholding and Support Vector Machine. *medRxiv*. https://doi.org/10.1101/2020.03.30.20047787.

[20] Hammoudi, K., H. Benhabiles, M. Melkemi, F. Dornaika, I. Arganda-Carreras, D. Collard, and A. Scherpereel. 2021. Deep Learning on Chest X-Ray Images to Detect and Evaluate Pneumonia Cases at the Era of COVID-19. *Journal of Medical Systems*. 45(7): 75. https://doi.org/10.1007/s10916-021-01745-4.

[21] Steve Eddins. 2013. "Homomorphic Filtering—Part 1."*Steve on Image Processing with MATLAB*. Accessed January 30, 2022. https://blogs.mathworks.com/steve/2013/06/25/homomorphic-filtering-part-1/.

[22] Wang, Zhi-She, Feng-Bao Yang, Zhi-Hao Peng, Lei Chen, and Lie Jin. 2015. Multi-Sensor Image Enhanced Fusion Algorithm Based on NSST and Top-Hat Transformation. *Optik*. 126(23): 4184–90. https://doi.org/10.1016/j.ijleo.2015.08.118.

[23] Jaeger, Stefan, Sema Candemir, Sameer Antani, Yì-Xiáng J. Wáng, Pu-Xuan Lu, and George Thoma. 2014. Two Public Chest X-Ray Datasets for Computer-Aided Screening of Pulmonary Diseases. *Quantitative Imaging in Medicine and Surgery*. 4(6): 475–77.

[24] Kumar, B., and O. Dikshit. 2017. Hyperspectral Image Classification Based on Morphological Profiles and Decision Fusion. *International Journal of Remote Sensing*. 38(20): 5830–54. https://doi.org/10.1080/01431161.2017.1348636.

[25] Yang, C., P. Liu, G. Yin, and L. Wang. 2017. Crack Detection in Magnetic Tile Images Using Nonsubsampled Shearlet Transform and Envelope Gray Level Gradient. *Optics & Laser Technology*. 90: 7–17. https://doi.org/10.1016/j.optlastec.2016.08.016.

[26] Yousif, A. S., U. U. Sheikh, and Z. Omar. 2019. A Novel Enhancement Method for Medical Image Using Double Density Wavelet and Stationary Wavelet Transforms. In *2019 IEEE 9th International Conference on System Engineering and Technology (ICSET)*. 292–97. https://doi.org/10.1109/ICSEngT.2019.8906378.

[27] Chavarín, Á., E. Cuevas, O. Avalos, J. Gálvez, and M. Pérez-Cisneros. 2023. Contrast Enhancement in Images by Homomorphic Filtering and Cluster-Chaotic Optimization. *IEEE Access*. 11: 73803–22. https://doi.org/10.1109/ACCESS.2023.3287559.

[28] Thakur, N., N. U. Khan, and S. Datt Sharma. 2022. Cuckoo Search Optimized Histogram Equalization for Low Contrast Image Enhancement. In *Proceedings of the 7th International Conference on Parallel, Distributed and Grid Computing (PDGC)*. 727–32. https://doi.org/10.1109/PDGC56933.2022.10053265.

[29] Yousif, A. S., Z. Omar, U. U. Sheikh, and S. A. Khalid. 2021. A Novel Pathological Stroke Classification System Using NSST and WLEPCA. In *2020 IEEE-EMBS Conference on Biomedical Engineering and Sciences (IECBES)*. 565–69. https://doi.org/10.1109/IECBES48179.2021.9398808.

[30] Khan, A. I., J. L. Shah, and M. M. Bhat. 2020. CoroNet: A Deep Neural Network for Detection and Diagnosis of COVID-19 from Chest X-Ray Images. *Computer Methods and Programs in Biomedicine*. 196: 105581. https://doi.org/10.1016/j.cmpb.2020.105581.

[31] Rahman, T., M. E. Chowdhury, A. Khandakar, K. R. Islam, K. F. Islam, Z. B. Mahbub, *et al.* 2020. Transfer Learning with Deep Convolutional Neural Network (CNN) for Pneumonia Detection Using Chest X-Ray. *Applied Sciences*. 10(9): 3233. https://doi.org/10.3390/app10093233.

[32] Randieri, C., A. Perrotta, A. Puglisi, M. G. Bocci, and C. Napoli. 2025. CNN-Based Framework for Classifying COVID-19, Pneumonia, and Normal Chest X-Rays. *Big Data and Cognitive Computing*. 9(7): 186. https://doi.org/10.3390/bdcc9070186.

[33] Oltu, B., S. Güney, S. E. Yuksel, and B. Dengiz. 2025. Automated Classification of Chest X-Rays: A Deep Learning Approach with Attention Mechanisms. *BMC Medical Imaging*. 25: 71. https://doi.org/10.1186/s12880-025-01604-5.